Integrated Modeling of Airborne Imaging Optical Sensors

Jun Ho Lee[1]*, Dongjun Choi[1], Chang Min Ok[2], Ho Jung[2], and Hyun Woo Park[2]

[1]Dept. of Optical Engineering, Kongju National University, Cheonan, South Korea
[2]Electro-Optics Research Center, LigNex1, Yongin, South Korea 16911
*jhlsat@kongju.ac.kr; phone +82-10-2633-9006; fax +82-41-521-9449; http://opticslab.kongju.ac.kr

***Abstract* - Airborne optical sensors are widely used in remote sensing applications, acquiring information about remotely located objects on a flying aircraft in optical electro-magnetic spectral bands. These sensors passively gather electro-magnetic (EM) radiation reflected or radiated by the object of interest or surrounding areas. The sensors record spatial and/or spectral information which arises on an electro-optical detector(s). Here, we develop a MATLAB-based simulation code which precisely predicts the formation of images by the optical sensors while considering all optical aspects of light propagation in sequence from the object through the atmosphere to the detector. This code is used to assess the impact of various operational conditions on the final image quality in terms of a modulation transfer function, the Strehl ratio and the bore-sight error. Sample results are presented for an airborne payload following a brief explanation of the theoretical models used in the imaging path.**

Keywords - optical sensor, remote sensing, imaging, simulation, integrated modeling, MTF, Strehl ratio

I. INTRODUCTION

An airborne optical sensor converts incoming light from objects at a distance into electronic signals in order to measure the physical quantity of light, which is then analyzed to understanding the object of interest [1]. Typical types of optical sensors include imaging optics, spectrometers and imaging spectrometers. The first records the spatial information, the second accounts for the spectral information, and the third collects both types [2-6]. Figure 1 shows optical concepts of an imaging camera and an imaging spectrometer.

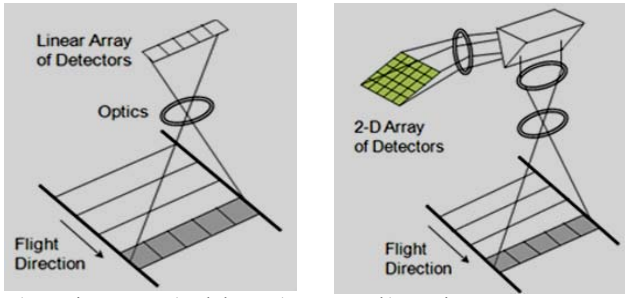

a) Imaging camera (push-broom) b) Imaging spectrometer

Figure 1. Optical concepts of imaging optics and an imaging spectrometer

For the imaging camera, it projects a strip of the earth surface onto a linear array of detectors through the imaging optics and it scans the surface as it flies over. Typically, the quality of images taken by airborne sensors can be predicted by a statistical tolerance analysis method called the root squared sum (RSS) method [7].

$$T \approx \sqrt{\sum_{i=1} t_i^2} \qquad (1)$$

where, T is the standard deviation of the entire system, t_i denotes the standard deviation of the ith part and n is the number of parts. In optics, T and t_i are most commonly described in terms of the root-mean-squared wavefront error (RMS WFE). Other important optical performance criteria, such as the MTF (modulation transfer function), can be predicted from the RMS wavefront error as follows,

$$\Delta MTF = k\,\Delta\ \ (\text{RMS WFE}) \qquad (2)$$

where k is a constant which depends on the detailed optics design; it is approximately 0.6 for typical airborne imaging cameras.

However, the RSS method is occasionally criticized considering its worst-case predictions. In addition, a statistical approach cannot properly consider realistic operational conditions, such as time-varying atmospheric disturbances through which light travels, aero-optic effects around the optical window on the sensor, sensor platform (aircraft) motion instability, and integration and noise effects of the detector.

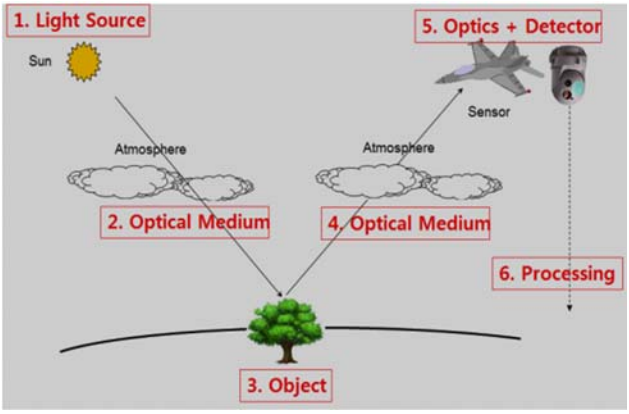

Figure 2. Schematic diagram of light propagation in airborne imaging

We are currently developing a MATLAB-based simulation code which precisely predicts image formation outcomes by optical sensors while considering all optical aspects of light propagation in sequence from the object through the atmosphere to the detector, i.e., from No. 3 to No. 5 in Figure 2. This code is used to assess the impact of various operational conditions on the final image quality in terms of the Strehl ratio, the MTF and the bore-sight error, i.e., the degree of geometrical accuracy.

The remainder of the paper is organized as follows. Section 2 presents an overview of the simulation code. Section 3 describes some of the mathematical models used for simulation operations, such as beam propagation through the atmosphere, the optical window, and image formation by an imaging optics with some exemplary results. Finally, Section 5 presents a few conclusive comments.

II. Simulation Overview

A simulation was conducted to model beam propagation and image formation from the object to the optical detector. The code considers the following principal features in sequence, referred to here as layers in the simulation model. We apply optical beam propagation from the object to the imaging optics using a phase-screen method and geometrical ray-tracing techniques [8], after which we apply Fourier optics and convolution techniques to generate the simulated object images [9].

- Object feature and radiant/reflective spectrum
- Atmospheric turbulence
- Aero-optics effect
- Optical window deformation
- Image formation

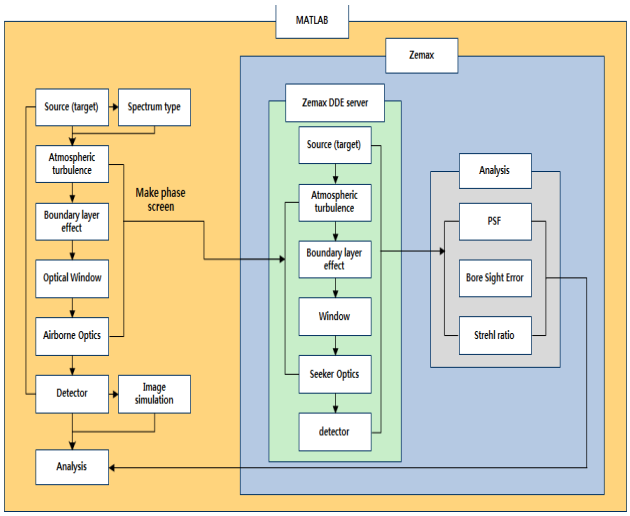

Figure 3. Overall architecture of the imaging simulation code

Figure 3 shows the overall architecture of the simulation code. The simulation code is written in a programming language called MATLAB developed by MathWorks [10] with an embedded internal link to optics design/analysis software called Zemax [11].

This code initially generates phase screens in MATLAB and then models them as sequential optical surfaces in Zemax. Optical calculations, in this case ray tracing, are then carried out inside Zemax, with these results fed back to MATLAB. Based on the results, MATLAB performs additional analysis processes such as image formation, and bore-sight error and MTF estimations.

III. Simulation Models

A. Beam Propagation

The phase-screen method considers the continuous medium as a series of thin lenses or diffraction screens that are orthogonal to the principal direction of propagation. The method implies that each phase screen induces a phase change abruptly at each screen position, as described by the following equations.

$$\mathrm{U}_{i+\Delta}(\mathrm{x},\mathrm{y}) = \mathrm{U}_i(\mathrm{x},\mathrm{y}) \times P_i(x,y) \tag{3}$$

$$P_i(x,y) \quad = A_i(x,y)\exp(i\emptyset_i(x,y)) \tag{4}$$

where, $\mathrm{U}_i(\mathrm{x},\mathrm{y})$ and $\mathrm{U}_{i+\Delta}(\mathrm{x},\mathrm{y})$ are the optical fields immediately before and after encountering the i[th] phase screen $P_i(x,y)$. $A_i(x,y)$ and $\emptyset_i(x,y)$ are the amplitude and phase functions of the i[th] phase screen, respectively, and the z-axis is the beam-propagation axis.

In this method, the beam is assumed to freely propagates between phase screens, as expressed by the following equation. This is known as the angular spectrum method [9].

$$\mathrm{U}_{i+1}(\mathrm{x},\mathrm{y}) = \mathrm{F}^{-1}\left\{ e^{i\sqrt{k^2-k_T^2}\Delta z} F\{\mathrm{U}_{i+\Delta}(\mathrm{x},\mathrm{y})\} \right\} \tag{5}$$

In this equation, F and F^{-1} are the Fourier transform and the inverse Fourier transform, respectively, and Δz is the distance between the i[th] phase screen and the next (i+1)[th] phase screen. k and k_T are the wavenumber and transverse wavenumber of the optical fields, respectively. In addition to this angular spectrum method, we can apply a geometrical ray-tracing technique to the transporting beams from layer to layer. As long as the integrated phase errors are smaller than a few waves, as usual, the geometrical approach results in faster calculations without scarifying the accuracy.

B. Atmospheric Turbulence

Computer simulations of atmospheric disturbances are commonly carried out based on several assumptions, including the presence of thin layers, the use of Kolmogorov statistics for phase aberrations, weak turbulence, and the frozen flow hypothesis [13, 14].

First, an atmospheric phase disturbance (i.e., a phase screen) at a single instance ($t=t_0$) is generated over an area much larger than the optics aperture. One of the most commonly utilized methods is the power spectrum method for simulating random phase screens from the Kolmogorov structure function,

$$\Phi(k) = 0.0229\, r_0^{5/3}\, k^{-11/3} \tag{6}$$

where r_o is the Fried parameter. The temporal evolution is predicted based on the frozen flow hypothesis [15]. Figure 4 shows the concept of the frozen flow hypothesis.

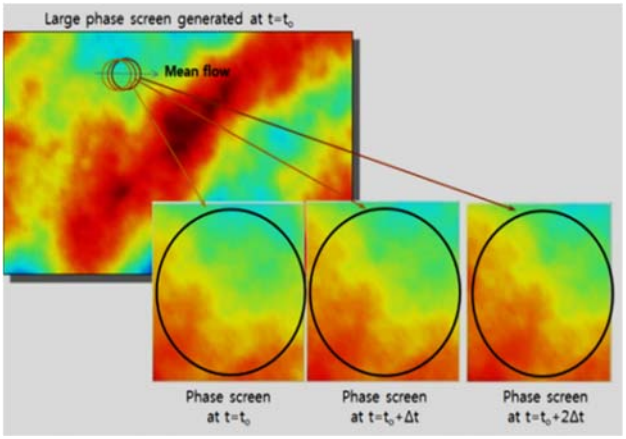

Figure 4. Concept of the frozen flow hypothesis

C. Aero-Optics Effect

An additional optical disturbance is induced by the turbulent flow field surrounding the optical sensor. The optical disturbance can be predicted via the Gladstone-Dale relationship [16],

$$n = 1 + K_{GD} \times \rho \tag{7}$$

$$K_{GD} = 2.23 \times 10^{-4}\left(1 + \frac{7.52\times10^{-3}}{\lambda^2}\right) \tag{8}$$

where n is the refractive index, K_{GD} is the Gladstone-Dale constant, and ρ denotes the air density distribution of the flow field. The air-density distribution (ρ) is solved by computational fluid dynamics software.

D. Optical Window

Every optical sensor has a transparent optical window. The window experiences mechanical deformation and a temperature gradient due to the surrounding temperature and pressure changes along with the air drag [17]. We apply the finite element analysis (FEA) initially to determine the window deformation and temperature distribution over the given operational conditions. From these results, we can determine the optical path length difference (OPD) over the full window area along the beam propagation, as shown below.

$$\mathrm{OPD}_{window}(x,y) = \int_{s1}^{s2} \frac{dn}{dT}\Delta T\, ds \tag{9}$$

where, T is the temperature and ΔT denotes the temperature difference.

The optical path difference in phase ($\phi_{window}(x,y)$) is then analyzed using the Zernike polynomial decomposition method over the beam aperture [18]. The optical field of the equivalent phase screen for the window (P_{window}) is then reconstructed as shown below:

$$P_{window}(x,y) = A_{window}(x,y)e^{i\phi_{window}(x,y)} \tag{10}$$

$$\phi_{window}(x,y) = \sum_{i=2} a_i Z_i(x,y) \tag{11}$$

$$a_i = \frac{1}{\pi}\frac{1}{A}\int OPL_{window}(x,y)Z_i(x,y)dxdy \tag{12}$$

In these equations, A is the area of the beam. The first Zernike polynomial Z_1, referred to as the piston, is excluded from the phase calculation in equation (11). Figure 5 shows a schematic diagram of the analysis flow.

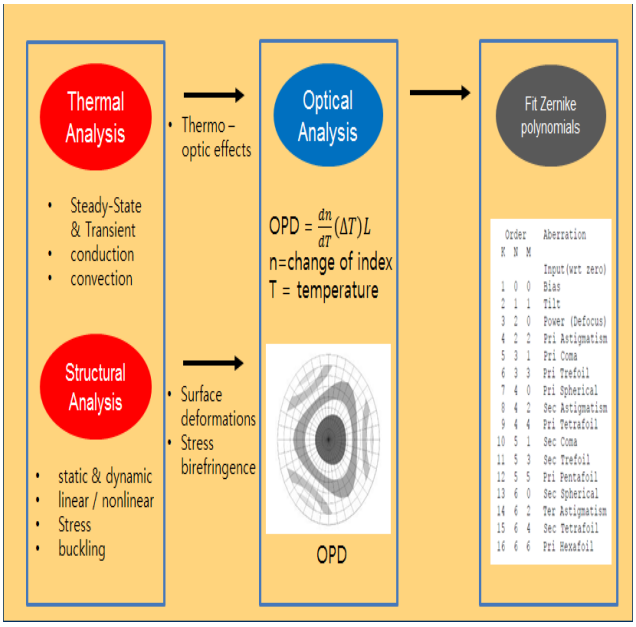

Figure 5. Phase screen generation for the optical window by means of a finite element analysis

E. Image Formation

The far-field point spread function (PSF) in the frequency coordinate (f_x, f_y) is computed by the Fourier transform of the final optical field U arriving at the entrance pupil of the optical sensor.

$$f_x = \frac{-r}{F\lambda} \quad (13)$$

$$f_y = \frac{-s}{F\lambda} \quad (14)$$

$$PSF(f_x, f_y) = \iint \; dxdy\, U(x,y) e^{-i2\pi(f_x x + f_y y)} \quad (15)$$

where, F is the focal length of the imaging camera and (r, s) denotes the position coordinates on the detector plane.

F. Some Results

Figures 6 to 8 show phase screens generated along the beam path with the following conditions or results:

- Atmospheric disturbance r_0=10cm
- FEA analysis results of an optical window with a 50 cm diameter

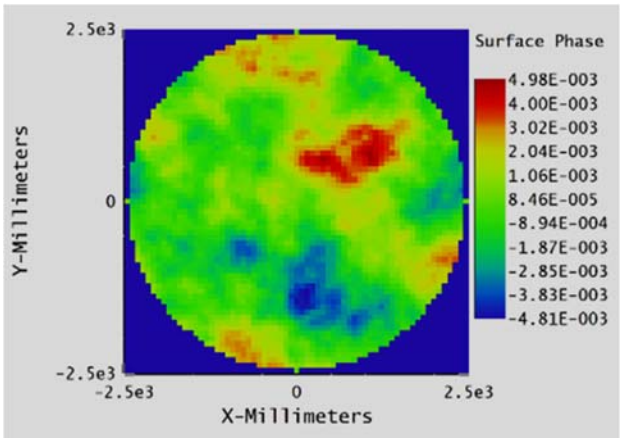

Figure 6. Computer-generated phase screen for an atmospheric disturbance of r_o=10 cm

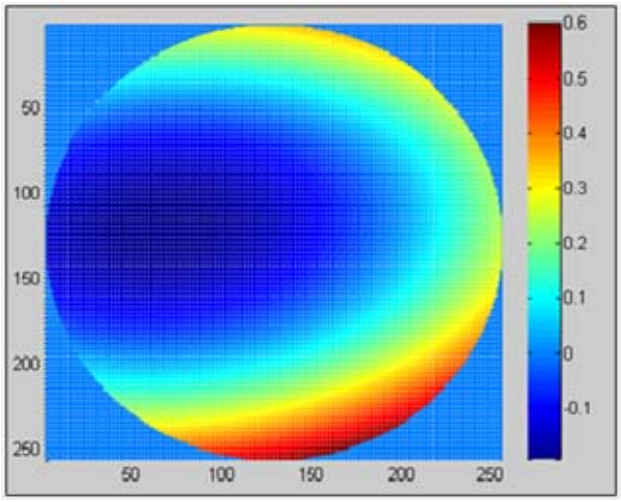

Figure 7. OPD screen for an optical window generated from a FEA analysis

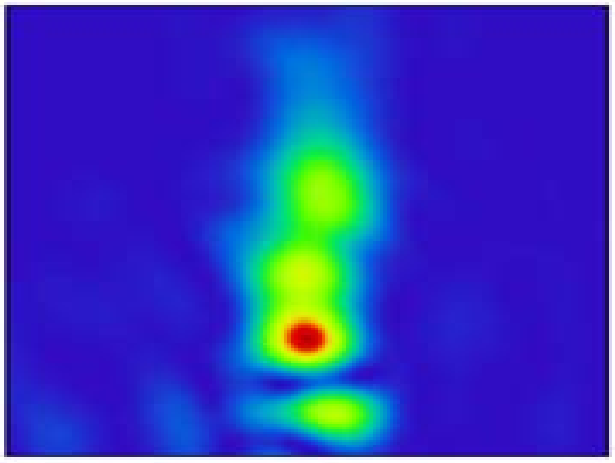

Figure 8. Resultant asymmetric PSF

IV. CONCLUSION

We are currently developing an image simulation code for air-borne optical sensors. The code is a MATLAB-based simulation code internally linked with the optical analysis/design software Zemax. The code models image formation of an airborne sensor using the phase-screen method. In this method, we model the beam propagation in sequence from the object through the atmosphere to the detector as phase screens.

The code is fully integrated but still in the verification phase. In a trial run, we combined the code with FEA results of an optical window.

Currently, we are considering further improvements of the current code combined with a scene model and a dynamic flight simulation model. These efforts can be used to study dynamic maneuvering effects on image quality levels and geometric location accuracy outcomes. Figure 9 shows the possible schematic configuration of the combined code.

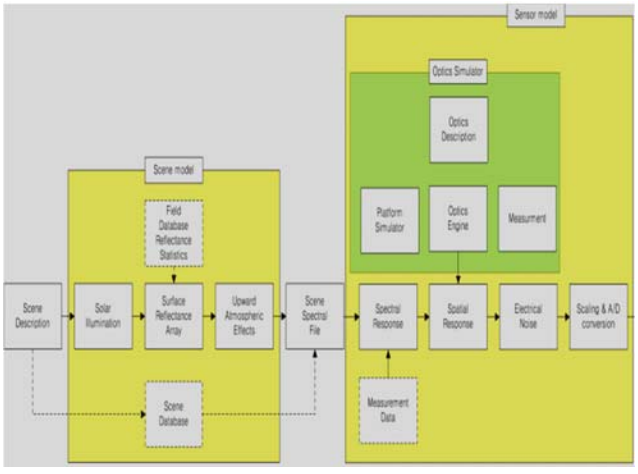

Figure 9. Schematic configuration of the imaging simulation code combined with a dynamic flight maneuvering simulation code.

ACKNOWLEDGEMENT

This work was supported by LIG Nex1.

REFERENCES

[1] J. B. Campbell and R. H. Wynne, Introduction to Remote Sensing, 5th ed., The Guilford Press, 2011.
[2] J. R. Wertz and W. J. Larson (Eds.), Space Mission Analysis and Design, 2nd ed., Space Technology Library, 1992
[3] S. Qian (Ed), Optical Payloads for Space Missions, Wiley, 2015
[4] E. E. Kim et al., "A high-resolution multi-spectral imaging system for small satellites," Acta Astronaut., vol. 52, pp. 813–818, 2003.
[5] J. H. Lee et al., "Imaging performance analysis of an EO/IR dual band airborne camera," J. Opt. Soc. Korea, vol. 15, no. 2, pp. 174–181, 2011.
[6] J. H. Lee, K. I. Kang and J. H. Park, "A very compact imaging spectrometer for the micro-satellite STSAT3," Int." Int. J. Remote Sensing 32(14), pp. 3935–3946 (2011).
[7] R. R. Yoder Ed., Optomechanical Design, SPIE, Volume CR43, pp. 76-108, 1992
[8] C. Grimault, "A multiple phase screen techniques for electromagnetic wave propagation through random ionospheric irregularities," Radio Science 33 (3), pp. 595-605, 1998
[9] J. W. Goodman, "Introduction to Fourier optics", Roberts & Company, Englewood, Colorado, 2005
[10] https://www.mathworks.com/products/matlab.html
[11] http://www.zemax.com/
[12] S. K. Yang, et al., "Ray tracing simulation of aero-optical effect using multiple gradient-index layer," Proc. SPIE 9987, 99870R, 2016.
[13] R. G. Lane, A. Glindemann, and C. Dainty, "Simulation of a Kolmogorov phase screen," Waves in Random Media 2 (3), pp. 209-224, 1992.
[14] C. M. Harding, R. A. Johnston, and G. Lane, "Fast simulation of a Kolmogorov phase screen," Appl. Opt. 38, pp. 2161-2170, 1999.
[15] B. L. Ellerbroek, "First-order performance evaluation of adaptive-optics systems for atmospheric-turbulence compensation in extended-field-of-view astronomical telescopes," J. Opt. Soc. Am. A 11, pp. 783-805, 1994.
[16] J. H. Gladstone and T. P. Dale, "Researches on the refraction, dispersion and sensitiveness of liquids," Phil. Trans. Royal Soc. London 153, pp. 317–343, 1864.
[17] J.H. Lee, et al., "Imaging Performance Analysis of an EO/IR Dual-Band Airborne Camera," J. Opt. Sco. Kor. 15(2), pp. 174-181, 2011.
[18] R. J. Noll, ''Zernike polynomials and atmospheric turbulence,'' J. Opt. Soc. Am. 66, pp. 207–211, 1976.